Inorganic Chemistry

Article

pubs.acs.org/IC

Flux Growth and Magnetoresistance Behavior of Rare Earth Zintl Phase EuMgSn

Xiaowei Ma,[†] Jun Lu,[‡] Jeffrey B. Whalen,[‡] and Susan E. Latturner*[,†]

[†]Department of Chemistry and Biochemistry, Florida State University, Tallahassee, Florida 32306, United States

[‡]National High Magnetic Field Laboratory, Florida State University, Tallahassee, Florida 32306, United States

Supporting Information

ABSTRACT: Reactions of europium and tin in 1:1 Mg/Al mixed flux produce large crystals of EuMgSn. This phase crystallizes with the TiNiSi structure type in orthorhombic space group *Pnma* (a = 8.0849(7) Å, b = 4.8517(4) Å, c = 8.7504(8) Å, Z = 4, R_1 = 0.0137). The crystal structure features europium cations positioned between puckered hexagonal layers comprised of magnesium and tin atoms. Magnetic susceptibility measurements indicate the europium in this phase is divalent, which suggests that the compound is possibly valence-balanced as $Eu^{2+}Mg^{2+}Sn^{4-}$. However, EuMgSn is a metal as indicated by density of states calculations and electrical resistivity behavior. This phase exhibits antiferromagnetic ordering at T_N = 10.9 K at low field (100 G) and the ordering temperature decreases when a higher magnetic field is applied. ac magnetization and field dependence of resistivity at 4.2 K reveal that there is a spin reorientation at 2 T, in agreement with the metamagnetic transition shown in the dc magnetization versus field data. Temperature dependence of resistivity at 2.5 T indicates that EuMgSn has a large magnetoresistance up to −30% near its magnetic ordering temperature.

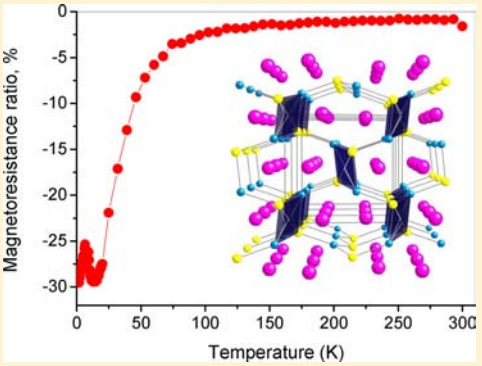

INTRODUCTION

Intermetallic compounds are traditionally synthesized by arc melting reactant elements with subsequent annealing at high temperatures. Unfortunately, the high temperatures employed promote the formation of thermodynamically favored products. Arc melting also allows very little control during the rapid heating and cooling of samples leading to polycrystalline products. The flux technique is an appealing alternative synthetic method for discovery and crystal growth of new phases.[1,2] This method involves the dissolution of solid reactants in a low-melting molten metal or salt, which helps to circumvent diffusion barriers. The lower reaction temperatures afforded by this technique can facilitate growth of kinetically stabilized phases, and slow cooling often leads to growth of large single crystals of products.[1−5] Using mixed fluxes composed of two elements can lower the melting point by eutectic formation, although it introduces additional complexity since one or both of the flux components may act as reactants and be incorporated into the products.

Previous research in our group has explored the use of several Mg-based molten Mg−X fluxes (X = Ni, Zn, Cu, Ga, Al) for the growth of new phases, with Mg/Al mixtures being of particular interest. The Mg/Al phase diagram exhibits a wide low melting range (40−60 atom % Mg, ∼450 °C) between the only two binary phases Mg_2Al_3 and $Mg_{17}Al_{12}$.[6] Mg/Al mixtures have proven to be good solvents for the synthesis of silicides such as CaMgSi and $R_5Mg_5Fe_4Al_{12}Si_6$ (R = Gd, Dy, Y).[7,8] However, it is difficult to distinguish Al and Si sites in the silicides containing aluminum because of their similar X-ray scattering cross sections. We therefore explored the replacement of silicon with its heavier congener tin in Mg/Al flux reactions. Stannides are more often sought using tin flux; some examples of phases grown in molten tin are Ti_2Sn_3,[9,10] Os_4Sn_{17},[11] $REMn_6Sn_6$ (RE = Tb, Ho, Er, Tm, Lu),[12] and $La_{4.87}Ni_{12}Sn_{24}$.[13] In this work, large EuMgSn single crystals were successfully grown in Mg/Al (and also Mg/Ag) flux. Although EuMgSn polycrystalline samples have previously been produced with traditional high temperature synthesis, the small crystal size limited the characterization of the phase and only powder X-ray diffraction data were reported.[14]

Europium intermetallic compounds have been widely studied due to the magnetic properties of the half-filled 4*f* shell of Eu^{2+} (variable Eu^{2+}/Eu^{3+} valence is also possible, but rare in intermetallics). Complex behavior is observed even in well-known and relatively simple structure types, as demonstrated by a review of the properties and partially polarized chemical bonding in 72 equiatomic EuTX compounds (T = transition metal; X = elements of groups 13, 14, or 15).[15] Europium is also being explored as a substitute for alkaline earth metals in Zintl phases; in compounds such as $Eu(Zn_{1-x}Ge_x)_2$ and EuGaSi, europium partially transfers valence electrons to the electronegative components leading to a pseudo gap at the Fermi level.[16−18] Such phases are of interest because changes in the magnetization of the rare earth ions may impact other physical properties such as the resistivity, potentially leading to

Received: December 22, 2012
Published: March 7, 2013

   dx.doi.org/10.1021/ic302828p | *Inorg. Chem.* 2013, 52, 3342−3348

magnetoresistance. For magnetoresistant materials, the electrical resistivity exhibits dramatic changes upon application of a magnetic field. EuMgSn appears to be close to a metal−insulator transition, as seen in the isostructural compound CaMgSi, which exhibits a metal to semimetal transition at ∼50 K.[7] Its resistivity is therefore very sensitive to perturbations caused by the magnetic ordering transition of the Eu^{2+} ions at 10 K. Introducing a magnetic ion into intermetallic phases that lie on the border between metallic and semiconducting behaviors appears to be a promising way of promoting magnetoresistivity.

EXPERIMENTAL SECTION

Synthesis. The elemental reactants were used as received: Mg and Al metal slugs (99.95%, Alfa Aesar), Ag crystalline powder (99.99%, Alfa Aesar), Sn metal slugs (99.9%, Cerac Inc.), and Eu slugs (99.9% Metall Rare Earth Ltd.).

The elements Mg/Al/Sn/Eu were initially weighed out in a 15/15/1/1 mmol ratio and loaded into a stainless steel crucible in an Ar-filled glovebox. The steel crucible was welded shut under argon and then sealed into a fused silica tube under vacuum (30 mTorr). The reaction ampule was placed in a muffle furnace and heated from room temperature to 950 °C in 10 h, held at 950 °C for 5 h, cooled to 750 °C in 80 h, and held at 750 °C for 24 h, at which point the reaction ampule was quickly removed from the furnace, flipped, and centrifuged to let the excess Mg/Al molten flux decant off the product crystals, which were adhered to the crucible wall. Reactions with different reactant ratios were compared to determine the highest yield, which was obtained at a Mg/Al/Sn/Eu ratio of 15:15:2:1. After the reaction ratio was optimized, the reaction was carried out in a niobium crucible to avoid the possibility of iron contamination; pure EuMgSn crystals could be grown by the same preparation method as stated above.

In addition to Mg/Al flux, Mg/Ag and tin fluxes were also explored as reaction media. The Mg/Ag eutectic (at 85/15 atomic% ratio) has a melting point of 450 °C, and reactions of the elements Mg/Ag/Sn/Eu in a mmol ratio of 17/3/2/1 were prepared using the same procedure described for Mg/Al flux. Tin has a very low melting point (232 °C) and reactions of Mg/Eu/Sn in a mmol ratio of 2/1/20 were prepared in alumina crucibles, sealed in fused silica tubes, and heated to 850 °C, held at 850 °C for 5 h, cooled to 600 °C in 80 h, and held at 600 °C for 24 h, at which point the reaction ampule was quickly removed from the furnace, flipped and centrifuged.

Elemental Analysis. SEM-EDS analysis was performed using a JEOL 5900 scanning electron microscope (30 kV acceleration voltage) equipped with PGT Prism energy dispersion spectroscopy software. Selected crystals were arranged on double-sided carbon tape adhered to an aluminum sample puck. Each crystal was cleaved to expose inner portions to acquire more accurate elemental analysis and avoid erroneous readings due to residual flux coating on the surface. Several spots on each crystal were analyzed for 60 s.

X-ray Diffraction. Single crystal diffraction data were collected at room temperature on a Bruker APEX2 single crystal diffractometer with a Mo Kα radiation source. Selected crystal samples were broken into suitable size and small spheroid fragments were mounted on glass fibers for the data collection. Data were processed using the program *SAINT* and corrected with the *SADABS* program.[19] Space group assignment was accomplished by *XPREP*, and refinement of the structure was performed using *SHELXTL*.[20] The structure of EuMgSn was solved in orthorhombic space group *Pnma*. In the final refinement cycles, occupancies of all sites were allowed to vary, but all appeared fully occupied (100 ± 1%). Crystallographic data and collection parameters are shown in Table 1 and important interatomic distances in Table 2; further data can be found in the CIF file in the Supporting Information. Powder X-ray diffraction data for crystals grown in Mg/Al and Mg/Ag fluxes were collected on a PANalytical X'Pert PRO diffractometer equipped with a Cu Kα radiation source. To prevent oxidation, samples were ground and loaded into an airtight holder inside a glovebox.

Table 1. Crystallographic Data and Collection Parameters for EuMgSn

cryst syst	orthorhombic
space group	*Pnma*
cell parameters, Å	a = 8.0849(7)
	b = 4.8517(4)
	c = 8.7504(8)
atom positions	Eu (0.01061(3), 1/4, 0.69129(2)); Mg (0.1523(1), 1/4, 0.0695(1)); Sn (0.27654(3), 1/4, 0.39392(3))
V, Å^3	343.24(5)
Z	4
calcd. density (g/cm^3)	5.71
max. 2θ (°)	56.56
radiation	Mo Kα
temperature (K)	290
reflns	3587
unique reflns	458
data/params	458/20
μ (mm^{-1})	25.26
R (int)	0.0232
R_1/wR_2[a] ($I > 2(I)$)	0.0137/0.0290
R_1/wR_2 (all data)	0.0142/0.0291
largest diff peak and hole (e·Å^{-3})	0.830/−1.128

[a] $R_1 = \Sigma(|F_o| - |F_c|)/\Sigma|F_o|$; $wR_2 = [\Sigma[w(F_o^2 - F_c^2)^2]/\Sigma(w|F_o|^2)^2]^{1/2}$.

Table 2. Interatomic Distances in EuMgSn

bond	bond distances, Å
Eu−Sn	3.3754(4), 3.4395(3), 3.4627(3)
Eu−Mg	3.464(1), 3.502(1), 3.687(1), 3.801(1)
Eu−Eu	4.1378(3), 4.1710(5), 4.8517(4)
Sn−Mg	2.9284(9), 3.011(1), 3.055(1)

TGA-DSC Measurement. Thermal analysis was performed on a SDT-Q600 (TA Instruments). EuMgSn crystals were ground into powder to increase the contact area with the alumina sample holder. The sample was heated to 1000 °C in 10 °C/min and then cooled to room temperature in argon atmosphere (100 mL/min). Powder X-ray diffraction data were collected on the thermally treated sample. Because a small endothermic peak was observed at around 430 °C, another EuMgSn sample was heated to just above that temperature (500 °C) in 10 °C/min and cooled down, and powder XRD data collected on the sample residue.

Electronic Structure Calculations. Density of states data for EuMgSn were calculated with the tight binding − linear muffin tin orbitals − atomic sphere approximation (TB-LMTO-ASA) program package.[21] The calculation was based on the EuMgSn structure parameters determined by single crystal X-ray diffraction data. The europium 4*f* electrons were treated as core electrons to avoid complications from partially filled shells in the calculation. Four types of empty Wigner-Seitz spheres in the radii range of 1.26−1.39 Å were added to fill the empty space in the structure. The following radii of atomic spheres were used: R(Eu) = 3.88 Å, R(Mg) = 2.98 Å, R(Sn) = 3.35 Å. The basis set contains Eu (6s, 5p), Mg(3s, 3p), and Sn (5s, 5p) with Eu(6p), Mg(3d), and Sn (5d, 4f) being downfolded. The calculation was made for 585 κ points in the irreducible Brillouin zone. Integration over the Brillouin zone was performed by the tetrahedron method.[22]

Magnetic Susceptibility. Magnetic susceptibility measurements were undertaken on a Quantum Design SQUID Magnetic Property Measurement System. Crystals grown in Nb crucibles were selected and held between two 4 cm long strips of kapton tape to eliminate background effects; this was placed in a straw attached to the sample holder. Temperature-dependent susceptibility data were collected

dx.doi.org/10.1021/ic302828p | *Inorg. Chem.* 2013, 52, 3342−3348

between 1.8 and 300 K at 100 G, 1000 G, 1.5 T, 2 and 2.5 T, respectively. Field-dependent magnetization data were collected at 4.2 K using applied fields up to 7 T. Magnetic anisotropy was studied by orienting the crystal with its *b* axis either parallel or perpendicular to the applied field. The field dependence of ac magnetic susceptibility was performed with 1 Hz frequency and 3×10^{-4} T amplitude of the ac field under a dc bias field up to 7 T.

Electrical Resistivity. Electrical resistivity measurements were conducted with a conventional four-probe method on a Physical Property Measurement System (PPMS) by Quantum Design. A single crystal (5 mm ×0.6 mm ×0.5 mm) was put on a sample holder puck and four 25 μm diameter gold wires were adhered to the crystal surface with silver paste. Resistivity data were taken from 1.9–300 K at 0 and 2.5 T with an applied excitation current of 0.5 mA. Field dependence of resistivity data were obtained at 4.2 K in the field range of 0–7 T. The magnetoresistance ratio (MR) at an applied field *B* was calculated using the equation $MR = \{[\rho(B) - \rho(0\ T))]/\rho(0\ T)\} \times 100$.

RESULTS AND DISCUSSION

Synthesis. Single crystals of EuMgSn in rodlike shape (up to 1 mm in diameter and 5 mm in length) were successfully grown in Mg/Al flux. The SEM image of a selected crystal is shown in Figure 1. The crystal surface appears clean indicating

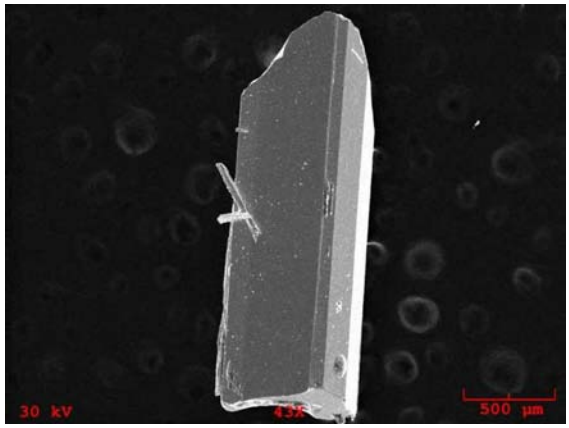

Figure 1. SEM image of a single crystal of EuMgSn grown from Mg/Al flux.

that most of the flux residue has been removed from the crystal by centrifugation at high temperature (750 °C). If lower centrifugation temperatures are used, the flux is more viscous and difficult to remove. The EuMgSn compound is air-sensitive and will darken if exposed to air for more than a day. The optimal Mg/Al/Sn/Eu reaction ratio is 15/15/2/1 leading to a 60% yield based on Eu. Aluminum was not incorporated into the structure and acts only as a flux component to enhance reactant solubility and diffusion. Attempts to make EuMgTt analogs with lighter tetrelides (via reactions such as Mg/Al/Tt/Eu where Tt = Si or Ge) lead instead to large crystals of the $Eu_{5+x}Mg_{18-x}Tt_{13}$ phases recently reported by Slabon and Nesper et al.[23]

EuMgSn can also be synthesized in Mg/Ag flux through the reaction of Mg/Ag/Sn/Eu (17/3/1/1 mmol ratio), although the yield is lower and the crystals smaller than those grown in Mg/Al flux. Powder X-ray diffraction data collected on products from Mg/Al and Mg/Ag fluxes are shown in Figure 2. No obvious impurity peaks are observed when compared with the calculated pattern. Attempts to form EuMgSn from reactions of europium and magnesium in tin flux produced the binary phase

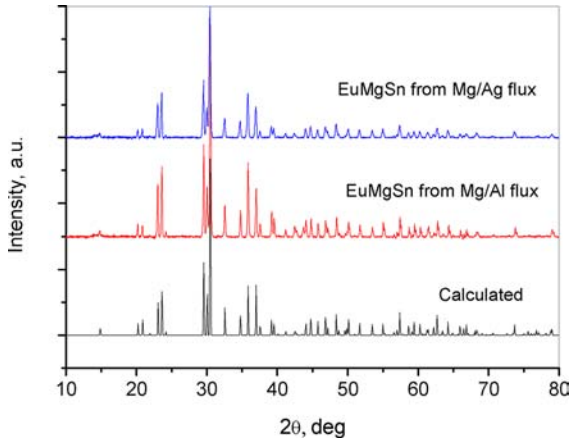

Figure 2. Powder X-ray diffraction patterns of EuMgSn samples from Mg/Al and Mg/Ag fluxes compared to calculated pattern based on single crystal structure.

$EuSn_3$, which was likely favored by the presence of the large amount of tin.

To determine whether EuMgSn melts congruently, TGA-DSC analysis was performed; the data are shown in Figure S1 of the Supporting Information. An endothermic peak appears at 910 °C during the heating process. The recrystallization of the sample occurs upon cooling to 800 °C indicated by an exothermic peak. However, powder X-ray data (Figure S2 of the Supporting Information) reveals that the sample has converted to mainly EuSn (small amounts of $EuSn_3$ and Sn were also present) after the thermal treatment. The ~6.5% weight loss above 910 °C is likely caused by the decomposition of the sample and associated vaporization of magnesium content (magnesium has a high vapor pressure and accounts for ~8% mass of EuMgSn). A tiny endothermic peak is also present at about 430 °C, which is likely attributed to melting of a small amount of Mg/Al flux on the crystal surface. The powder X-ray data of another EuMgSn sample heated only to 500 °C does not exhibit any difference from the original powder pattern, as shown in Figure S2 of the Supporting Information, indicating that this peak does not correspond to a phase change.

Structure. EuMgSn crystallizes with the common TiNiSi structure type (orthorhombic space group *Pnma*), isostructural to EuZnSn,[24,25] EuPdSn, and EuPtSn.[26,27] Atom positions are listed in Table 1. The structure of EuMgSn is shown in Figure 3 (viewed down the *b* axis). Each type of atom occupies only one site in the structure. Magnesium and tin atoms alternate and are connected to form puckered hexagonal layers along the *bc* plane, and neighboring layers are connected by rhombic Mg_2Sn_2 units (as highlighted in blue) along the *a* axis. Magnesium and tin atoms are each coordinated by a distorted tin or magnesium tetrahedron, respectively. A comparison of atom positioning in the anionic frameworks of the stannides EuMgSn, EuZnSn, EuPdSn, and EuPtSn shows different sitings for the tin atoms. The Sn sites in the Mg/Sn and Zn/Sn frameworks correspond to Pd (or Pt) sites in the Pd/Sn (or Pt/Sn) frameworks. This phenomenon results from the higher electronegativity of Sn than Mg or Zn, in contrast to Sn having lower electronegativity than Pd (or Pt).[15] The Mg–Sn intralayer distances of 2.9284(9) Å and 3.011(1) Å in the Mg_3Sn_3 hexagons are slightly shorter than the Mg–Sn bond distance of 3.055(1) Å between the layers. Considering the sum

dx.doi.org/10.1021/ic302828p | Inorg. Chem. 2013, 52, 3342–3348

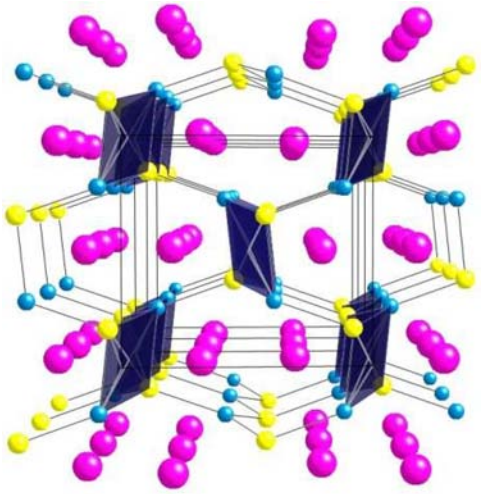

Figure 3. Structure of EuMgSn viewed down the *b* axis; europium, magnesium, and tin atoms are pink, yellow, and cyan, respectively.

of the metallic radii of 2.79 Å for magnesium and tin,[28] the Mg−Sn intralayer bonds are more covalent than the Mg−Sn interlayer bonds. While magnesium is an alkaline earth metal, it behaves more like a transition metal in EuMgSn, similar to zinc in EuZnSn.

Europium ions, the most electropositive species in the structure, reside between the puckered Mg/Sn layers. Each europium atom is sandwiched by two puckered Mg_3Sn_3 hexagons leading to a coordination of Eu by 6 magnesium atoms and 5 tin atoms within the range of 3.3754(4) Å to 3.801(1) Å. One tin atom is located farther (4.096 Å) from the europium and hence is excluded. Inspection of the distances between europium ions in EuMgSn indicates that each is adjacent to six other Eu ions, with two of them located along the *b* direction at a distance of 4.1378(3) Å and two more further out at 4.8517(4) Å; the other two are at a distance of 4.1710(5) Å along the *a* direction. The two sets of neighboring europium ions at distances of 4.1378(3) and 4.1710(5) Å likely cause competing magnetic interactions observed in magnetic studies discussed later.

Electronic Structure Calculations. Figure 4 exhibits the calculated total and partial density of states (DOS) diagram for EuMgSn. Not surprisingly, the DOS data for EuMgSn resembles that reported for isostructural and isoelectronic CaMgSi.[7] A pseudogap (~1.3 states eV^{-1} per unit cell) at the Fermi level (E_F) reveals that EuMgSn is still metallic, and not semiconducting as would be expected for a charge-balanced Zintl phase ($Eu^{2+}Mg^{2+}Sn^{4-}$). The DOS analysis agrees well with the electrical resistivity of EuMgSn, which shows behavior typical of a metal (vide infra). Electropositive europium has the main contribution to the states above the E_F, whereas tin states are predominant below the E_F. Magnesium states are highly disperse in a wide range across the E_F indicating strong hybridization with Eu and Sn states. Eu, Mg, and Sn elements all contribute to the states near E_F indicating a significant cation−anion orbital overlap. While modeling of Eu^{2+} *f*-states was not possible, they are known to be located near the Fermi level in intermetallics facilitating phenomena such as valence fluctuation and 4*f*−5*d* hybridization.[29] This allows the partially delocalized valence electrons of europium to impact the electrical conductivity when a magnetic field is applied as is discussed in the resistivity section.

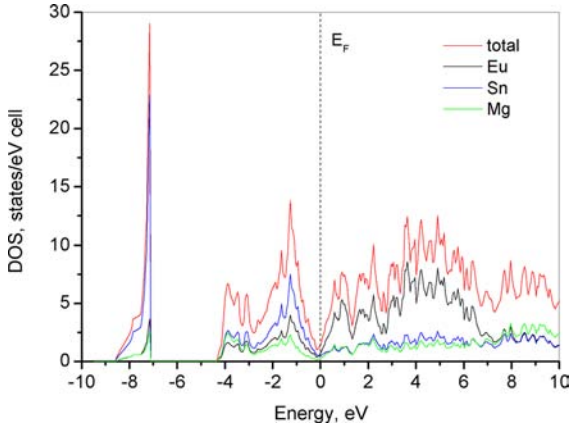

Figure 4. Partial and total density of states data calculated for EuMgSn.

Magnetic Properties. Magnetic measurements were performed on a EuMgSn single crystal prepared in a Nb crucible, with its *b* axis oriented either parallel or perpendicular to the magnetic field. The parallel magnetic susceptibilities versus temperature of EuMgSn (ZFC and FC) at 100 G, 1000 G, 1.5 T, 2 T, and 2.5 T are shown in part a of Figure 5. All curves indicate antiferromagnetic transitions with decreasing Néel temperature (T_N) as higher field is applied. As seen from part a of Figure 5, EuMgSn has a T_N = 10.9 K at 100 G and a T_N of 7.8 K at 2.0 T. When the field increased to 2.5 T, the susceptibility below 6 K was almost saturated, and T_N is difficult to see. The shifts of Néel temperature toward low temperature is attributed to the nature of the antiferromagnetic transition.[30] An external magnetic field applied parallel to the easy axis of a structure (*b* axis for EuMgSn) creates a force that competes with the antiferromagnetic exchange interactions, destabilizing the antiferromagnetic ordering and driving the Neel temperature lower. If the external field is large enough, the europium moments will be induced to align with it, and a spin flop to a ferromagnetic state can occur.

This field-induced spin reorientation can also be seen in field-dependent magnetization measurements performed at 4.2 K with the *b* axis of the crystal aligned both parallel and perpendicular to the field (Figure 6). When the field is applied parallel to the *b* axis, the magnetization versus field displays linear behavior up to 2 T, at which point a metamagnetic transition occurs. This transition is also evidenced by the χ' peak at H_{cr} = ~2 T in the ac magnetization as a function of the applied dc field (Figure 7). A second peak is present at ~2.6 T revealing the spin reorientation is almost complete at that field. Figure 6 also displays the magnetization data for the crystal with *b* axis perpendicular to the applied field, and the magnetization increases linearly with increasing field over the entire field range to 7 T. The magnetization in both orientations starts to saturate at 7 T.

The inverse magnetic susceptibility versus temperature curves of EuMgSn (insets in Figure 5) can be fit to the Curie−Weiss law above 50 K resulting in effective magnetic moments per europium ion of 7.9−8.4 μ_B. The theoretical magnetic moments of Eu^{2+} and Eu^{3+} are 7.9 and 3.4 μ_B respectively. Hence, europium ions in EuMgSn have a +2 oxidation state. The positive sign of the Weiss constant (θ = 3 K) indicates that ferromagnetic coupling forces are present at high temperatures, which contradicts the observed antiferro-

dx.doi.org/10.1021/ic302828p | Inorg. Chem. 2013, 52, 3342−3348

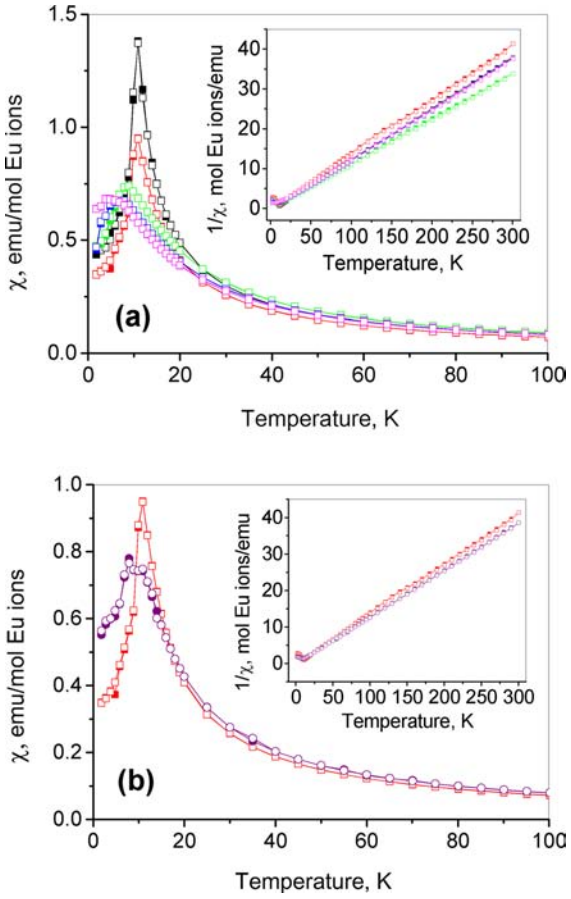

Figure 5. Temperature dependence of magnetic susceptibility for EuMgSn. (a) Data for crystal oriented with *b* axis parallel to the applied field, taken at different fields (data for 100 G, 1000 G, 1.5 T, 2 T, 2.5 T are black, red, green, blue, magenta). Solid and empty squares are for zero field cooled (ZFC) and field cooled (FC) data respectively. Inset: $1/\chi$ vs *T*. (b) Data for crystal oriented with *b* axis parallel (red) or perpendicular (purple) to the field taken at 1000 G. Solid and empty squares are for zero field cooled (ZFC) and field cooled (FC) data respectively. Inset: $1/\chi$ vs *T*.

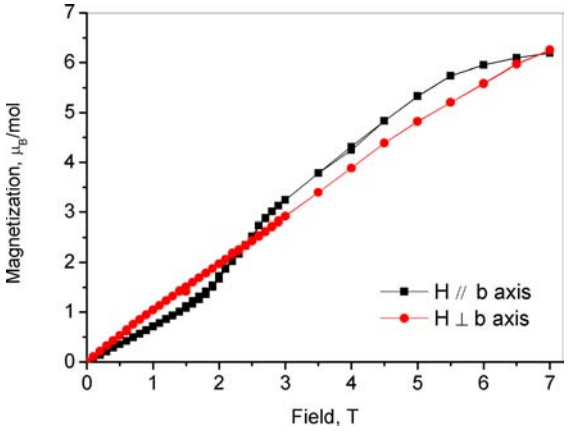

Figure 6. Field dependence of magnetization at 4.2 K for EuMgSn crystal oriented with *b* axis either parallel or perpendicular to the field.

magnetic ordering. There are evidently two competing mechanisms for ordering, which is also supported by the observation of the spin reorientation in Figures 6 and 7. As shown in Figure 3, each Eu^{2+} ion has six neighboring Eu^{2+} ions

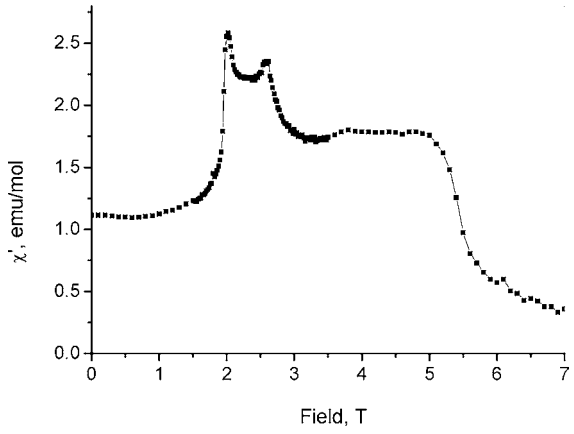

Figure 7. Field dependence of ac magnetization of EuMgSn at 4.2 K (ac frequency 1 Hz).

at distances of 4.1378(3) Å, 4.1710(5) Å, and 4.8517(4) Å along the *a*, *b*, and *c* axes respectively, which will lead to competing coupling forces.

To study the magnetic anisotropy of EuMgSn, magnetic susceptibility measurements were also undertaken with the *b* axis of the crystal oriented perpendicular to the applied 1000 G magnetic field and the result is shown in part b of Figure 5. For the convenience of comparison, the parallel magnetic susceptibility at 1000 G is also included. Although the two curves are very similar, the parallel susceptibility shows a higher Néel temperature (10.9 K) compared to the perpendicular one (7.9 K), indicative of the *b* axis as the easy axis. The straight $1/\chi$ versus *T* curve at above T_N follows Curie–Weiss law very well, and the calculated effective magnetic moment (7.9 μ_B) is similar to that found for the parallel orientation.

Resistivity and Magnetoresistance. Standard four-probe resistivity measurements were undertaken in the temperature range 1.9–300 K. To study the magnetoresistance of EuMgSn, the measurements were also carried out at an applied field of 2.5 T. These data are shown in Figure 8. At temperatures above ~100 K, the difference between zero-field resistivity and that at 2.5 T is negligible, and the resistivity decreases almost linearly with decreasing temperature, typically indicative of metallic behavior. The resistivity of EuMgSn at 300 K (3.8×10^{-6} Ω·m) lies in the metallic range (10^{-7}–10^{-1} Ω·m),[31] and it is several

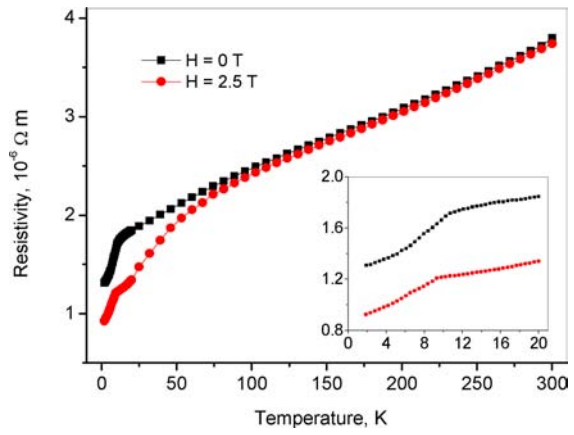

Figure 8. Temperature dependence of the electrical resistivity of EuMgSn crystal at both 0 and 2.5 T applied fields. Inset: Low temperature data.

dx.doi.org/10.1021/ic302828p | Inorg. Chem. 2013, 52, 3342–3348

orders of magnitude smaller than that of CaMgSi (1.95×10^{-2} Ω·m),[7] consistent with the expected trend of metallicity increasing as Ca is replaced by Eu and as Si is replaced by Sn. At temperatures below ∼100 K, a divergence between the sample resistivity at 2.5 T and at zero field can be observed (that is, magnetoresistance). Under an applied field, resistivity drops in a sharper slope until the magnetic ordering temperature of ∼9.3 K, at which point the resistivity falls rapidly to 9.2×10^{-7} Ω·m at 1.9 K. In the zero field case, the resistivity decreases at a constant rate until a slope change appears at the ordering temperature of ∼10.2 K.

Traditionally, compounds with metallic conductivity do not show significant magnetoresistance; metals usually have a magnetoresistance ratio (MR) of less than 2%.[32] However, colossal magnetoresistance is often associated with materials that exhibit competing magnetic interactions with associated metamagnetic transitions, or compounds that are close to a metal−insulator transition. EuMgSn exhibits both these characteristics; the structure has two slightly different and competing Eu−Eu interactions, and an ostensibly semiconducting stoichiometry with a pseudo gap at the Fermi level. This results in a large MR of −29.5% at 12 K and an applied field of 2.5 T. The effect of similar competing magnetic interactions is evidenced in EuMgAu and EuMgAg phases (also with the TiNiSi structure), which also exhibit magnetoresistance.[33] This effect will be heightened in EuMgSn by the presence of the pseudogap at E_F putting the phase close to a metal−insulator transition (which was observed for isostructural and isoelectronic CaMgSi).[7] For rare earth Zintl phases with a pseudo gap, the few electronic states at the Fermi level provide sufficient mobile electrons to produce metallic conductivity. However, if the localized magnetic moments of the Eu^{2+} cations are strongly coupled with the conduction electrons, magnetoresistance can occur when the 4f moments order. Accordingly, colossal magnetoresistance has been observed in several rare earth Zintl phases, such as $EuIn_2M_2$ (M = As, P), $EuGa_2M_2$ (M = As, P), and $Eu_xCa_{1-x}B_6$, with $EuIn_2P_2$ exhibiting a negative MR of −298% at a temperature of 24 K and applied field of 5 T.[34−36]

The temperature dependence of the magnetoresistance of EuMgSn was calculated from the resistivity versus temperature data at zero field and 2.5 T and is shown in Figure 9. The magnitude of the magnetoresistance ratio increases drastically as the temperature falls below 100 K, with a maximum of −29.5% at 12−16 K. This is consistent with the report that the highest MR value is often observed near the magnetic ordering temperature.[34,37] The field dependence of resistivity at 4.2 K (Figure 10) further indicates how resistivity is affected by the varying field. A valley with the minimal resistivity (1.16×10^{-6} Ω·m) is observed in the field range of 2.0−2.9 T; this is the range at which a metamagnetic transition is indicated by the dc and ac magnetization data shown in Figures 6 and 7. The peak magnetoresistance for EuMgSn is found at the combination of temperature and field that promotes a metamagnetic transition from an antiferromagnetic to ferromagnetic ordered state. The induced ferromagnetic ordering of europium spins reduces the effect of spin scattering on the conduction electrons, minimizing resistivity.

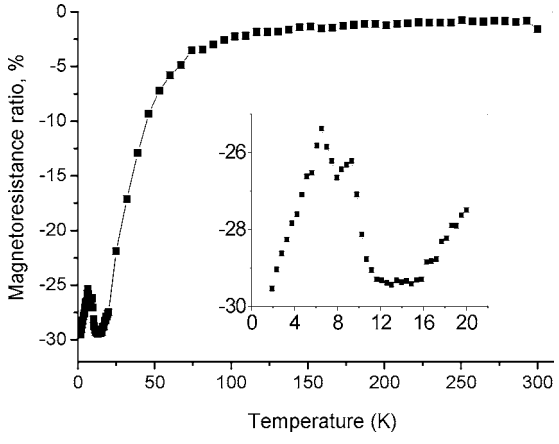

Figure 9. Temperature dependence of magnetoresistance ratio (MR) for EuMgSn at an applied field of 2.5 T. Inset: Low temperature data.

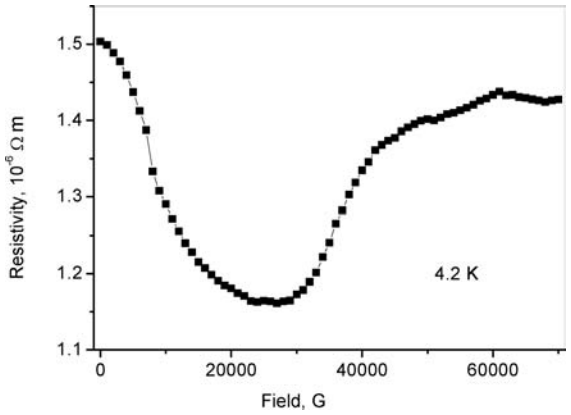

Figure 10. Field dependence of resistivity for EuMgSn at 4.2 K.

CONCLUSIONS

Reactions of tin and europium in Mg/Al (or Mg/Ag) flux have yielded large EuMgSn single crystals, which are difficult to obtain from traditional solid state synthesis. Although it is tempting to view EuMgSn as a rare earth Zintl phase based on the stoichiometry, DOS calculations and transport measurements reveal that it has metallic character with a pseudo gap at the Fermi level. The low number of carriers are likely coupled to the localized Eu^{2+} moments and strongly scattered by them. Therefore, reducing spin scatter by inducing a ferromagnetic ordering of these moments will have a large effect on the resistivity of the compound. Accordingly, large magnetoresistance is observed at low temperature and applied fields sufficient to force a metamagnetic transition from antiferromagnetic to ferromagnetic ordering.

ASSOCIATED CONTENT

Supporting Information

TGA and DSC data, powder X-ray diffraction for thermally treated EuMgSn residue, and crystallographic data for EuMgSn in the form of CIF files. This material is available free of charge via the Internet at http://pubs.acs.org.

AUTHOR INFORMATION

Corresponding Author

*E-mail: latturne@chem.fsu.edu, phone: 850-644-4074, fax: 850-644-8281.

Notes

The authors declare no competing financial interest.

dx.doi.org/10.1021/ic302828p | Inorg. Chem. 2013, 52, 3342−3348

■ ACKNOWLEDGMENTS

This research was supported by funding from the National Science Foundation (Division of Materials Research) through grant numbers DMR-05-47791 and DMR-11-06150; the NHMFL facilities are supported by DMR-06-54118 and the state of Florida.

■ REFERENCES

(1) (a) Kanatzidis, M. G.; Pöttgen, R.; Jeitschko, W. *Angew. Chem., Int. Ed.* **2005**, *44*, 6996−7023. (b) Phelan, W. A.; Menard, M. C.; Kangas, M. J.; McCandless, G. T.; Drake, B. L.; Chan, J. Y. *Chem. Mater.* **2012**, *24*, 409−420.
(2) Bugaris, D. E.; zur Loye, H. C. *Angew. Chem., Int. Ed.* **2012**, *51*, 3780−3811.
(3) Ribeiro, R. A.; Avila, M. A. *Phil Mag.* **2012**, *92*, 2492−2507.
(4) Mahjoor, P.; Latturner, S. E. *Phil Mag.* **2012**, *92*, 2582−2595.
(5) West, J. P.; Hwu, S. J. *J. Solid State Chem.* **2012**, *195*, 101−107.
(6) Massalski, T. B.; Okamoto, H. *Binary Alloy Phase Diagrams*, 2nd ed.; ASM International: Materials Park, OH, 1990.
(7) Whalen, J. B.; Zaikina, J. V.; Achey, R.; Stillwell, R.; Zhou, H. D.; Wiebe, C. R.; Latturner, S. E. *Chem. Mater.* **2010**, *22*, 1846−1853.
(8) Ma, X. W.; Chen, B. H.; Latturner, S. E. *Inorg. Chem.* **2012**, *51*, 6089−6095.
(9) Kleinke, H.; Waldeck, M.; Gütlich, P. *Chem. Mater.* **2000**, *12*, 2219−2224.
(10) Künnen, B.; Jeitschko, W.; Kotzyba, G.; Mosel, B. D. *Z. Naturforsch. B.* **2000**, *55*, 425−430. Erratum: Künnen, B.; Jeitschko, W.; Kotzyba, G.; Mosel, B. D. *Z. Naturforsch. B.* **2000**, *55*, 887.
(11) Lang, A.; Jeitschko, W. *J. Mater. Chem.* **1996**, *6*, 1897−1903.
(12) Clatterbuck, D. M.; Gschneidner, K. A., Jr. *J. Magn. Magn. Mater.* **1999**, *207*, 78−94.
(13) Zhuravleva, M. A.; Bilc, D.; Mahandi, S. D.; Kanatzidis, M. G. *Z. Anorg. Allg. Chem.* **2003**, *629*, 327−334.
(14) Merlo, F.; Pani, M.; Fornasini, M. L. *J. Alloys Compd.* **1993**, *196*, 145.
(15) Pöttgen, R.; Johrendt, D. *Chem. Mater.* **2000**, *12*, 875−897.
(16) Bobev, S.; Bauer, E. D.; Thompson, J. D.; Sarrao, J. L.; Miller, G. J.; Eck, B.; Dronskowski, R. *J. Solid State Chem.* **2004**, *177*, 3545−3552.
(17) You, T. S.; Grin, Y.; Miller, G. J. *Inorg. Chem.* **2007**, *46*, 8801−8811.
(18) You, T. S.; Lidin, S.; Gourdon, O.; Wu, Y. Q.; Miller, G. J. *Inorg. Chem.* **2009**, *48*, 6380−6390.
(19) *SAINT*, Version 6.02a, Bruker AXS, Inc.: Madison, WI, 2000.
(20) Sheldrick, G.M. *SHELXTL NT/2000*, Version 6.1; Bruker AXS, Inc.: Madison,WI, 2000.
(21) Jepsen, O.; Burkhardt, A.; Andersen, O. K. *The Program TB-LMTO-ASA, version 4.7*; Max-Planck-Institut fur Festkorperforschung: Stuttgart, Germany, 2000.
(22) Blöchl, P. E.; Jepsen, O.; Andersen, O. K. *Phys. Rev. B* **1994**, *49*, 16223−16233.
(23) Slabon, A.; Cuervo-Reyes, E.; Kubata, C.; Mensing, C.; Nesper, R. *Z. Anorg. Allg. Chem.* **2012**, *638*, 2020−2028.
(24) Merlo, F.; Pani, M.; Fornasini, M. L. *J. Less-Common Met.* **1991**, *171*, 329.
(25) Pöttgen, R. *Z. Kristallogr.* **1996**, *211*, 884.
(26) Pöttgen, R. *Z. Naturforsch.* **1996**, *51b*, 806.
(27) Adroja, D. T.; Malik, S. K. *Phys. Rev.* **1992**, *45B*, 779.
(28) Pauling, L. *The Nature of the Chemical Bond and the Structure of Molecules and Crystals*; Cornell University Press: Ithaca, NY, 1960.
(29) Szytula, A.; Leciejewicz, J. *Handbook of Crystal Structures and Magnetic Properties of Rare Earth Intermetallics*. CRC Press, Boca Raton, 1994.
(30) Carlin, R. L. *Magnetochemistry*; Springer-Verlag, Berlin, NY, 1986.
(31) West, A. R. *Basic Solid State Chemistry*, 2nd ed.; John Wiley & Sons, Ltd.: Chichester, West Sussex, England, 1999.
(32) (a) Chan, J. Y.; Kauzlarich, S. M.; Klavins, P.; Shelton, R. N.; Webb, D. J. *Chem. Mater.* **1997**, *9*, 3132−3135. (b) Chan, J. Y.; Kauzlarich, S. M.; Klavins, P.; Shelton, R. N.; Webb, D. J. *Phys. Rev. B* **1998**, *57*, R8103−R8106.
(33) Hartmann, H.; Berggold, K.; Jodlauk, S.; Klassen, I.; Kordonis, K.; Fickenscher, T.; Pöttgen, R.; Freimuth, A.; Lorenz, T. *J. Phys.: Condens. Matter* **2005**, *17*, 7731−7741.
(34) (a) Goforth, A. M.; Klavins, P.; Fettinger, J. C.; Kauzlarich, S. M. *Inorg. Chem.* **2008**, *47*, 11048−11056. (b) Jiang, J.; Kauzlarich, S. M. *Chem. Mater.* **2006**, *18*, 435.
(35) Goforth, A. M.; Hope, H.; Condron, C. L.; Kauzlarich, S. M.; Jensen, N.; Klavins, P.; MaQuilon, S.; Fisk, Z. *Chem. Mater.* **2009**, *21*, 4480−4489.
(36) Wigger, G. A.; Beeli, C.; Felder, E.; Ott, H. R.; Bianchi, A.; Fisk, Z. *Phys. Rev. Lett.* **2004**, *93*, 147203−1.
(37) Bauhofer, W.; McEwen, K. A. *Phys. Rev. B.* **1991**, *43*, 13450.